Int J Adv Manuf Technol (2000) 16:773–783
© 2000 Springer-Verlag London Limited

The International Journal of
Advanced
Manufacturing
Technology

A 3D Predictive Cutting-Force Model for End Milling of Parts Having Sculptured Surfaces

T. S. Lee and Y. J. Lin

Department of Mechanical Engineering, University of Akron, Ohio, USA

A comprehensive, 3D mathematical model of desired/optimal cutting force for end milling of freeform surfaces is proposed in this paper. A closed-form predictive model is developed, based on a perceptive cutting approach, resulting in a cutting force model having a comprehensive set of essential cutting parameters. In particular, the normal rake angle, usually missing in most existing models of the same sort, is included in the developed model. The model also permits quantitative analyses of the effect of any parameters on the cutting performance of the tool, providing a guideline to improving the tool performance. Since the axial depth of cut varies with time when milling sculptured surface parts, an innovative axial depth of cut estimation scheme is proposed for the generation of 3D cutting forces. This estimation scheme improves on the practicality of most existing predictive cutting-force models for milling, in which the major attention has been focused on planar milling surface generation. In addition, the proposed model takes the rake surface on the flute of mills as an osculating plane to yield 3D cutting force expressions in only two steps. This approach greatly reduces the time-consuming mathematical work normally required for obtaining the cutting-force expressions. A series of milling simulations for machining freeform parts under specific cutting conditions have been performed to verify the effectiveness of the proposed cutting-force model. The simulation results demonstrate the accurate estimating capability of the proposed method for axial depth of cut estimation. The cutting force responses from the simulation exhibit the same trends as can be obtained using the empirical mechanic's model referenced in the literature. Finally, from the simulation results it is also shown that designing a tool with a combination of different helix angles, having cutting force signatures similar to those of the single helix angle counterparts, is particularly advantageous.

Keywords: Cutting force; Machining; Sculptured surface

Correspondence and offprint requests to: Dr Y. J. Lin, Department of Mechanical Engineering, University of Akron, Akron, OH 44325–3903, USA. E-mail: yl@uakron. edu

1. Introduction

One of the most common metal removal operations used in industry is the milling process. The current practice of milling sculptured surface parts is to choose overly conservative cutting conditions so that excessive cutting forces or deflection of the cutter do not occur [1]. However, as a high material removal rate is mandated, the preferable way is to generate optimal cutting conditions before actual machining. To realise this, a comprehensive mathematical model for surface milling is required. Since cutting force is the most important output parameter of end milling that has direct influence on the quality of machined parts, developing an accurate cutting-force model is essential.

Prediction of end-milling forces is not a new area in manufacturing industry. However, most of the literature focuses on 2D cases where the contribution of the axial force to the dynamic behaviour of the cutter is missing. Although a few 3D cutting-force models have been developed recently, they have inherent shortcomings which merit further research in the area.

In this paper, a more accurate and comprehensive 3D cutting-force model for end milling, including sculptured surface cutting, is proposed. The physical shape of the end milling cutter, as in most other similar work, is assumed to be a cylinder with helical flutes wound around its surface. However, the proposed model takes the rake surface of a flute to be an osculating plane, as opposed to viewing it as a ruled surface as in most existing models. With this new approach, the expressions of the unit vectors of a local right-handed orthonormal curvilinear coordinate system become simple, compact, and well defined. Consequently, the unit tangent vector always points in the direction of increasing spread angle, the unit principal normal is directed toward the origin of the cutter, and the direction of the unit bi-normal always points outward and is perpendicular to the rake surface. The direct benefit of this proposed approach is that the loading distribution on a flute owing to the pressure of the chip on each elemental cutting edge can be simplified to be a single resultant force. Also, the location of the line of action of the force can be determined by applying the principle of moments. Thus, the

magnitude of the resultant force is equal to the sum of all the elemental forces acting on the flute at that instant of cut.

The second consideration is of sculptured surface machining. It is found that, so far, cutting force modelling for sculptured surface milling has not attracted much attention. Since, along a path of cut for generating a sculptured surface, the axial depth of cut varies, the cutting-force determination is, therefore, based mainly on the updated axial depth of cut estimation. For this purpose, an innovative method for varying axial depths of cut estimation has been proposed in this paper.

Lastly, it has been reported that helix angle is one of the most important parameters in influencing the cutting-force dynamics of a milling cutter [2]. Within the proposed cutting-force model, the total cutting-force equations derived are aimed at being more versatile, because the model allows various helix angles of the flutes to be incorporated in the cutting-force equations. Therefore, the proposed model can be used to assist the design of an optimal milling cutter which is composed of flutes with different helix angles for special needs.

2. Related Works

Cutting-force modelling of end milling has been investigated extensively; [3–8] are some recent representative works. However, these investigations resulted in either prediction only for static cutting forces which induce errors in realistic machining, or models leading to less accurate cutting-force prediction owing to a lack of physical comprehension. For example, Smith and Tlusty [3] developed a model called the average rigid force model in which the average power required for a cut was assumed to be proportional to the metal removal rate. The force model is inaccurate because it does not include the influence of the cutter geometry and cutting conditions.

In 1994, Bayoumi et al. [4,5] developed a 3D mechanistic force model. They used the ruled surface method to describe the rake surfaces of the flutes of the cutter. As a result, the expressions for the unit vectors of the moving trihedron of the flutes become complicated and the directions of the vectors are not well defined. In addition, to emulate cutting forces accurately, each differential helical cutting-edge segment of the flute is viewed as an oblique tool with an inclination angle equal to the helix angle. The approach resulted in cumbersome mathematical expressions for the cutting forces which not only depend on the geometry of the cutter, normal rake angle, and helix angle, but also on the process-dependent parameters such as chip load (feed) and angular position of the chip.

The mechanistic force modelling method has also been investigated by several researchers. Sabberwal [9] suggested that the cutting force on the flute of a cutter is mainly due to the tangential part of the force, and the force is proportional to the undeformed chip area removed by that flute from the region of engagement between the cutter and workpiece. Martellotti [10] found that the contour generated by a cutting flute can be considered to be circular. He then formulated the chip load as $f \bullet \sin\theta$, where f is the feed of the cut and θ is the angular position of the cutter. It has become the most frequently employed expression for the chip load. Tlusty and MacNeil [11], and King [12] adopted a similar expression for tangential force, and further assumed that radial force is related to the tangential force by a constant coefficient. Kline et al. [13] and DeVor et al. [14] developed a discrete mechanistic force model in which the chip along each flute of the cutter is divided into a series of discrete thin disks. Similar to the model used by Tlusty and MacNeil, the elemental cutting forces contributed by each disk can be calculated. The total cutting forces are then obtained by summing all these elemental cutting forces numerically. Based on this force model, Kline and DeVor [15] examined the effects of the cutter runout on the cutting forces. Sutherland and DeVor [16] took a step further. In addition to the cutter runout, they also incorporated static deflection of the cutter into their cutting force model. Later, Sutherland [17] improved the cutting force model presented in [16] by taking the dynamic nature of the cutter deflection into consideration. The main drawback of this discrete mechanistic force method is that, at each instant of time, new discrete chip disks must be obtained from the new cutting region. This requires that the cutting forces be recalculated numerically. Therefore, it is a computationally intensive method. It can be found that all the models discussed above were 2D force models, which are unable to predict cutting force in the axial direction. This motivated the development of the first 3D mechanistic force model, proposed by Bouzakis et al. [18] in 1985. Their model was also formulated in a discrete form. Therefore, it can be expected that the model inherited the same drawbacks as those of the 2D discrete models.

Other researchers such as Armarego and Deshpande [19] used the mechanics of the cutting approach to predict milling cutter forces. They began with partitioning the cutting edge of each tooth into a series of differential elements. By viewing each of these differential cutting edges as an oblique cutting tool, they used the cutting force equations derived by Armarego and Brown [20]. However, the accuracy of the predicted cutting forces by this method relies entirely on the quality of the input data including such parameters as shear stress and normal shear angle, etc. Unfortunately, this parameter information is generally not available in the literature.

3. Three-Dimensional Cutting Force Formulation

In this section, a comprehensive 3D cutting force model for the end-milling process is proposed. The model is derived based on the assumption that the formation of the chip is of a continuous type. In addition, the model assumes that the tool is perfectly sharp and rigid, and chattering, tool breakage, and wear do not occur during the course of machining.

The model is derived in four sequential steps and their procedures are:

1. Define unit vectors for a curvilinear coordinate system at any specified point of a flute. In differential geometry, the coordinate system at that specific point is called the trihedron or triad. However, as the point changes, the coordinate system moves along the flute. In this case, the system is known as the moving trihedron. The main function of this coordinate system is to describe the directions in which the cutting forces are exerted on the flute.

2. Derive expressions for the pressure and friction components of the cutting forces. The first component in the force model is due to the cutting chip pressing on the rake surface of the flute, and is known as the pressure component. The other part, called the friction component, is due to the sliding motion of the chip on the surface.
3. Establish the integration limits so that the cutting force equations can be formulated in a closed form format.
4. Develop a methodology for estimating the ever-changing depth of cut through machining of parts having sculptured surfaces.

These four sequential steps will be elaborated in the following subsections.

3.1 Unit Vector Representation of a Helical Flute

The geometric shape of a flat-end milling cutter is a right circular cylinder with the flutes of the cutter winding around the cylinder. The geometric shape of a flute is a circular helix. Figure 1 shows a typical flat-end milling cutter with flute i lying on the surface of the cutter. The cutter has a radius R and is rotated at a constant angular velocity ω. In order to describe instantaneous orientation and the position of a point on the flute, two sets of coordinate systems, namely, a fixed and a rotational coordinate system are required. Referring to Fig. 1, the coordinate system $x_0y_0z_0$ is the fixed coordinate system and $x_iy_iz_i$ is the rotational coordinate system. The main purpose of the rotational coordinate system is for describing the position of a point on a flute. For example, the instantaneous rotational orientation of a flute such as flute i, as shown in Fig. 1, can be described by the angle β_i, which is the angle between the x_i-axis of the rotational coordinate system $x_iy_iz_i$ and the x_0-axis of the fixed coordinate system. In defining this angle, the x_i-axis is established in such a way that it passes through the leading point on the cutting edge of the flute. From the geometry of the cutter as shown in Fig. 1, the position vector $\mathbf{r}_i$ for a point on the flute i that corresponds to the spread angle ψ_i is obtained as

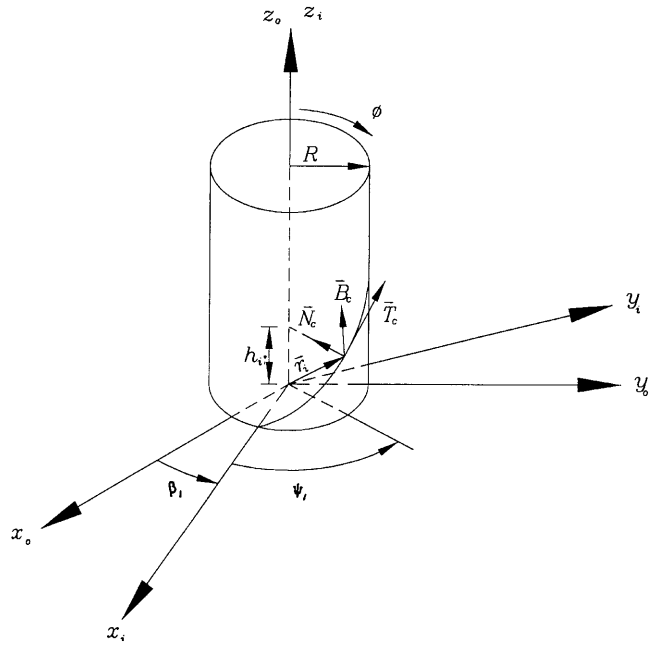

Fig. 1. Geometric description for a point on a flute.

$$\mathbf{r}_i = R\cos\psi_i\mathbf{e}_1 + R\sin\psi_i\mathbf{e}_2 + h_i\mathbf{e}_3 \tag{1}$$

where $\mathbf{e}_1$, $\mathbf{e}_2$, and $\mathbf{e}_3$ are the unit vectors pointed in the directions of the x_i-, y_i- and z_i-axes, respectively, and h_i is used to indicate the elevation of a point on the flute i. Because the geometric shape of the flute of the cutter is a circular helix, the elevation of a point on the flute is proportional to the circumferential movement, $R\psi_i$ of the cutter. Hence, the elevation of a point on the flute i at a spread angle ψ_i can be written as

$$h_i = R\psi_i \cot\alpha_i \tag{2}$$

where α_i is the helix angle of the flute i, i.e. the angle between the unit tangent $\mathbf{T}_c$ of the helical flute and the z_i-axis. In addition, to form a local righthanded rectangular coordinate system at each point of the flute, there are two other unit vectors required, namely, the unit normal $\mathbf{N}_c$ and bi-normal vector $\mathbf{B}_c$. This coordinate system is used to describe cutting forces acting on the cutting edges of the flute.

As can be seen in Eqs (1) and (2), the position vector is a function of the spread angle ψ_i. However, using the relation $s = \int|d\mathbf{r}_i/d\psi_i|d\psi_i$, the position vector of the flute can then be transformed into a function in which the arc length s is a variable. Therefore, applying the chain rule with the definition of unit tangent, $\mathbf{T}_c = d\mathbf{r}_i/ds$, and the relation that relates the derivative of arclength s to that of position vector, $ds/d\psi_i = |d\mathbf{r}_i/d\psi_i|$, the unit tangent can be expressed in terms of ψ_i as

$$\mathbf{T}_c = \frac{d\mathbf{r}_i}{ds} = \frac{d\mathbf{r}_i}{d\psi_i}\Big/\frac{ds}{d\psi_i} = \frac{d\mathbf{r}_i}{d\psi_i}\Big/\left|\frac{d\mathbf{r}_i}{d\psi_i}\right|$$

$$= -\sin\psi_i\sin\alpha_i\mathbf{e}_1 + \cos\psi_i\sin\alpha_i\mathbf{e}_2 + \cos\alpha_i\mathbf{e}_3 \tag{3}$$

As in the case of a unit tangent, the unit normal along the helical flute is also defined in terms of arclength s. However, using the chain rule and the relation $ds/d\psi_i = |d\mathbf{r}_i/d\psi_i|$, this quantity can also be expressed in terms of ψ_i. Therefore, the expression of the unit normal is given by

$$\mathbf{N}_c = \frac{d\mathbf{T}_c}{ds}\Big/\left|\frac{d\mathbf{T}_c}{ds}\right| = -\cos\psi_i\mathbf{e}_1 - \sin\psi_i\mathbf{e}_2 \tag{4}$$

Equation (3) indicates that $\mathbf{T}_c$ is tangent to the flute and pointed in the direction of increasing ψ_i. On the other hand, Eq. (4) implies that the vector $\mathbf{N}_c$ points toward the origin of the $x_iy_iz_i$ coordinate system and is parallel to the x_iy_i-plane.

The plane that contains vectors $\mathbf{T}_c$ and $\mathbf{N}_c$ is called an osculating plane. However, in metal cutting terms it is equivalent to the rake surface of the cutter. In fact, this is the surface from which the chip will be removed by the cutting operation.

With $\mathbf{T}_c$ and $\mathbf{N}_c$ defined, the unit bi-normal vector $\mathbf{B}_c$ required to complete the triplet of the local coordinate system can be obtained by applying the cross-product. Thus, it is perpendicular to the osculating plane, or can be expressed in terms of ψ_i as

$$\mathbf{B}_c = \mathbf{T}_c \times \mathbf{N}_c$$
$$= \sin\psi_i \cos\alpha_i \mathbf{e}_1 - \cos\psi_i \cos\alpha_i \mathbf{e}_2 + \sin\alpha_i \mathbf{e}_3 \quad (5)$$

After having defined the curvilinear coordinate system sufficiently, a closed-form mechanistic cutting-force model can then be developed.

3.2 Closed-Form Mechanistic Cutting Force Model

Figure 2 shows a flat-end milling cutter in the process of machining a slot in a workpiece. The cutter is fed in the direction of x_0 with a feedrate of f_r. The axial and radial depths of cut are d_a and d_r, respectively. As the cutter rotates with an angular velocity ω, a point on flute i will start engaging with the workpiece at an angular position equal to the cutter entry angle θ_{en} and will leave the cut at an angular position equal to θ_{ex}, the cutter exit angle. As depicted in Fig. 2, the instantaneous angular position of such a point with reference to the fixed coordinate system $x_0y_0z_0$ can be described by angle γ_i. The corresponding chip thickness h_c of the point is determined by the radial difference between paths 1 and 2 as follows:

$$h_c = f \cos\gamma_i \quad (6)$$

where f is the feed of the cutter.

As shown in Fig. 2, the cutter entry angle for a given radial depth of cut can be determined by

$$\theta_{en} = \sin^{-1}[d_r/R) - 1] \quad (7)$$

By cross-referencing Fig. 1 with Fig. 2, it can be seen that the instantaneous angular position γ_i of the point on the flute can now be written as $\gamma_i = \beta_i + \psi_i - \phi$ with β_i being the angular position of the leading point on the cutting edge of the flute i and ϕ being the instantaneous position of the cutter owing to the cutter rotation rate ω. If the cutter has more than one flute with the pitch between any two flutes being constant, then the angular position of the leading point can be shown to be $\beta_i = \beta_r + (i-1)(2\pi/N_f)$, where β_r is the angular position of the leading edge point of the referenced flute and i varies from 1 to N_f, $i = 1,2, \ldots N_f$.

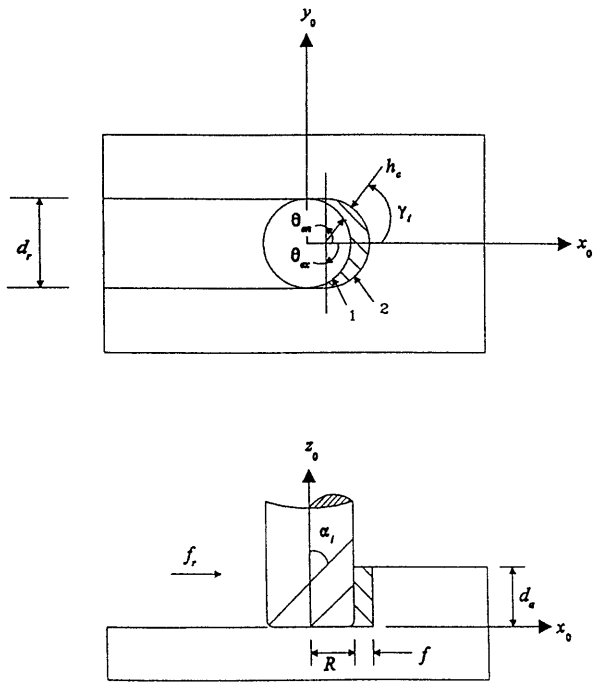

Fig. 2. Cut geometry and positive coordinate sign convention for a flat-end mill.

Figure 3 shows an elemental cutting edge of flute i. The axial depth of cut by this elemental cutting edge is dz_i. The cutting force acting between this elemental cutting edge and the work piece is dz_i. The cutting force acting between this elemental cutting edge and the workpiece can be resolved into two components: a pressure and a friction component. The pressure component acts in the direction perpendicular to the rake surface of the flute. This component provides a measure of the compressive action which the chip applies to the surface of the flute. However, the friction component is applied parallel to the surface owing to the sliding movement of the chip on the surface of the flute. Since the chip slides up the surface without any restraint on its movement, it is expected that the friction force would act in the direction of the chip movement.

For a flute with zero helix angle, the chip slides on the rake surface along the direction of $\mathbf{N}_c$. However, when the helix angle of the flute is greater than zero, the chip will take a path that makes an angle η_i with $\mathbf{N}_c$. Referring to Fig. 3 as well as to Eqs (3) and (4), the unit vector defining the direction of the chip movement on the rake surface of the flute can be found to be

$$\mathbf{Q}_c = \cos\eta_i \mathbf{N}_c + \sin\eta_i \mathbf{T}_c$$
$$= -(\cos\eta_i \cos\psi_i + \sin\eta_i \sin\psi_i \sin\alpha_i)\mathbf{e}_1$$
$$+ (\sin\eta_i \cos\psi_i \sin\alpha_i - \cos\eta_i \sin\psi_i)\mathbf{e}_2$$
$$+ \sin\eta_i \cos\alpha_i \mathbf{e}_3 \quad (8)$$

where η_i is called the chip flow angle. However, in the case when the information regarding this angle is not available, then as an approximation it is generally assumed to be equal to the helix angle of the flute, $\eta_i = \alpha_i$. In metal cutting, it is known as the Stabler's flow rule.

The dimensions of the chip which are required for calculating cutting forces are obtained from the projection of the elemental axial depth of cut dz_i and the undeformed chip thickness h_c in the direction of chip flow on the plane of the rake surface.

As shown in Fig. 3, the geometry of the chip movement shows the triangles *ADF* and *AFE* do not lie on the same plane. Triangle *ADF* is in the plane normal to the cutting edge, while triangle *AFE* lies on the plane of the rake surface. However, these two triangles share the same edge *AF*. Therefore, in order to find the length of the chip *AE* from the undeformed chip thickness $AD = h_c$, one must first project *AD* orthogonally onto *AF*, and then project *AF* back to *AE*. In the light of Eq. (6),

$$AE = \frac{AD}{\cos\epsilon_i \cos\eta_i} = \frac{f \cos\gamma_i}{\cos\epsilon_i \cos\eta_i} \quad (9)$$

where the angle ϵ_i is known as the normal rake angle formed between *AD* and *AF* and is located in the plane normal to the cutting edge. Similarly, the width *BC* of the chip can be obtained accordingly. It is noted that that triangles *ACB* and *AGB* do not lie on the same plane but they have the same

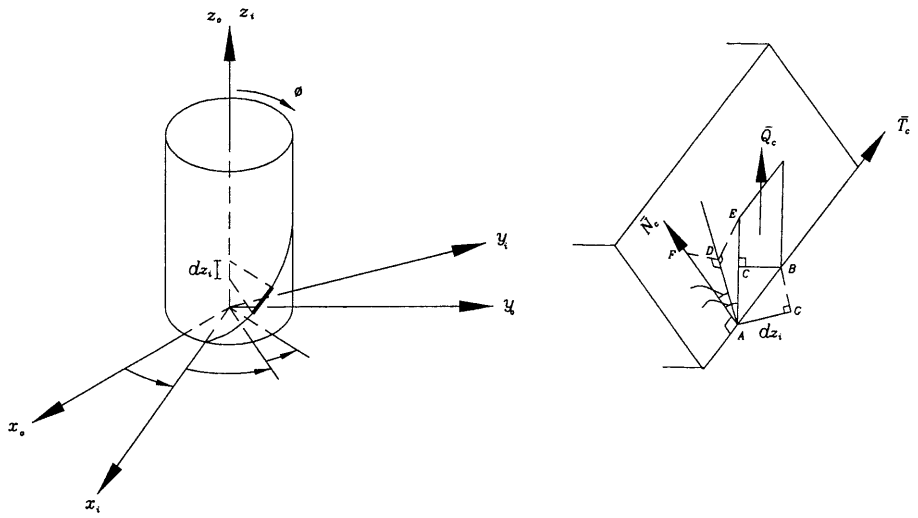

Fig. 3. Projection of the undeformed chip area into the direction of chip flow on a rake surface.

hypotenuse *AB*. Thus, from the geometry, the width of the chip *BC* can be expressed as

$$BC = AB\cos\eta_i = \frac{dz_i}{\cos\alpha_i}\cos\eta_i \tag{10}$$

where dz_i is the differential axial depth of cut for flute i at a differential spread angle $d\psi_i$. In analogy to Eq. (2), dz_i can be written as $dz_i = \mathrm{R}\ \cot\ \alpha_i d\psi_i$. Thus, the normal cutting force for this differential cutting edge can be written as:

$$d\,F_{i,p} = K_c\ (\mathrm{AE})\ (\mathrm{BC}) \tag{11}$$

where K_c is defined as the specific cutting pressure. It is a variable that depends on the material properties of the workpiece/tool and on the geometry of the tool as well as on the undeformed chip thickness.

After obtaining this elemental cutting force model, the cutting force due to the pressure component for the flute at an instant of cut can be predicted by summing up the elemental cutting forces at each elemental cutting edge of the flute. Substituting Eqs (9) and (10) into Eq. (11) and then integrating the resultant equations yields

$$F_{i,p} = \frac{fRk_c}{\cos\ \in_i \sin\alpha_i}\int_{\psi_{i,L}}^{\psi_{i,U}} \cos(\beta_i + \psi_i - \phi)d\psi_i$$

$$= \frac{fRK_c}{\cos\ \in_i \sin\ \alpha_i}\left[\sin(\beta_i + \psi_{i,U} - \phi) - \sin(\beta_i - \psi_{i,L} - \phi)\right] \tag{12}$$

where $\psi_{i,L}$ and $\psi_{i,U}$ are used to indicate the range of the cutting edge of the flute engaged with the workpiece. Applying the principle of moments yields

$$R\bar{\gamma}_i F_{i,p} = \int R\gamma_i\, \mathrm{d}F_{i,p} \tag{13}$$

where $\bar{\gamma}_i$ is the equivalent angular position for the line of action of $F_{i,p}$, usually denoted by $\bar{\gamma}_i = \beta_i - \phi + \psi_i$, with ψ_i being the equivalent spread angle.

Since the radius of the cutter R is a constant, substituting Eqs (11) and (12) into Eq. (13) gives

$$\bar{\psi}_i = \left[\frac{c_1 - c_2 + c_3 - c_4}{\sin(\beta + \psi_{i,U} - \phi) - \sin(\beta + \psi_{i,L} - \phi)}\right] - (\beta_i - \phi) \tag{14}$$

where the terms c_1, c_2, c_3, and c_4 are all constants having the following expressions:

$$c_1 = \gamma_{i,U}\sin(\beta_i + \psi_{i,U} - \phi)$$
$$c_2 = \gamma_{i,L}\sin(\beta_i + \psi_{i,L} - \phi)$$
$$c_3 = \cos(\beta_i + \psi_{i,U} - \phi)$$
$$c_4 = \cos(\beta_i + \psi_{i,L} - \phi)$$

in which $\gamma_{i,U}$ and $\gamma_{i,L}$ are $\gamma_{i,U} = \beta_i - \phi + \psi_{i,U}$ and $\gamma_{i,L} = \beta_i - \phi + \psi_{i,L}$, respectively.

Finally, the cutting force due to the pressure component in the local coordinate system becomes

$$\mathbf{F}_{i,p} = F_{i,p}\bar{B}_c = -F_{i,p}\sin\psi_i\cos\alpha_i\mathbf{e}_1 + F_{i,p}\cos\psi_i\cos\alpha_i\mathbf{e}_2 - F_{i,p}\sin\alpha_i\mathbf{e}_3 \tag{15}$$

where $\bar{B}_c$ is a unit binormal vector evaluated at the equivalent spread angle $\bar{\psi}_i$.

In addition, the frictional force can be written as

$$\mathbf{F}_{i,f} = K_f F_{i,p}\bar{Q}_c = -K_f F_{i,p}(\cos\eta_i\cos\psi_i + \sin\eta_i\sin\psi_i\sin\alpha_i)\mathbf{e}_1 + K_f F_{i,p}(\sin\eta_i\cos\psi_i\sin\alpha_i - \cos\eta_i\sin\psi_i)\mathbf{e}_2 + K_f F_{i,p}\sin\eta_i\cos\alpha_i\mathbf{e}_3 \tag{16}$$

where K_f is the coefficient of friction on the interface of the chip and the rake surface of the flute. In Eq. (15), $\bar{\mathbf{Q}}_c$ is used to indicate the evaluation of the unit chip flow vector at the equivalent spread angle $\bar{\psi}_i$.

However, summing the cutting force contributed by these pressure and friction components will yield the total local cutting force acting on the flute. Hence, the components of the total local cutting force are given by

$$F_{i,x} = -F_{i,p}\sin\bar{\psi}_i\cos\alpha_i - K_f F_{i,p}$$
$$(\cos\eta_i\cos\bar{\psi}_i + \sin\eta_i\sin\bar{\psi}_i\sin\alpha_i)$$
$$F_{i,y} = F_{i,p}\cos\psi_i\cos\alpha_i + K_f F_{i,p}(\sin\eta_i\cos\psi_i\sin\alpha_i - \cos\eta_i\sin\bar{\psi}_i)$$
$$F_{i,z} = -F_{i,p}\sin\alpha_i + K_f F_{i,p}\sin\eta_i\cos\alpha_i \quad (17)$$

Equation (17) is only applicable to a single flute force analysis. To obtain a global cutting force on the tool for a multiflute cutter, the global cutting force acting on the tool can be written as

$$\begin{Bmatrix} R_x \\ R_y \\ R_z \end{Bmatrix} = \sum_{i=1}^{N_e} \begin{bmatrix} \cos(\beta_i - \phi) & -\sin(\beta_i - \phi) & 0 \\ \sin(\beta_i - \phi) & \cos(\beta_i - \phi) & 0 \\ 0 & 0 & 1 \end{bmatrix} \begin{Bmatrix} F_{i,x} \\ F_{i,y} \\ F_{i,z} \end{Bmatrix} \quad (18)$$

where N_e is the number of cutter flutes involved in the cut at that instant of time. To use Eq. (18) as a model to predict the instantaneous cutting force on the tool, the data regarding the cutter specification, i.e. R, N_f, ϵ_i, α_i, and cutting conditions, i.e. d_a, d_r, f_r, f, as well as the cutting process parameters, i.e. K_c, K_f, η_i, must be available and be used as inputs to the model.

3.3 Integration Limits

The integration limits $\psi_{i,L}$ and $\psi_{i,U}$ for flute i depend on the cutter entry angle θ_{en} and the cutter exit angle θ_{ex}, as well as on the instantaneous angular position γ_i of a point on the flute. These variables in turn are functions of the radial and axial depths of cut, d_r and d_a, respectively, as well as on the angular position β_i of the leading edge point of the flute and the spread angle ψ_i for a point on the flute at a given axial depth of cut.

As shown in Fig. 4, at any instant of time, the rotational position of a flute can assume any one of the five possible positions. For example, in Fig. 4(*a*) where the leading edge point of the flute is located in the region *B* while the angular position $\gamma_{i,a}$ for the point on the flute corresponding to the axial depth of cut d_a is in region *A*, the integration limits for the flute at this orientation are $\psi_{i,L} = 0$ and $\psi_{i,U} = \theta_{en} - (\beta_i - \phi)$, respectively, where the expression for $\gamma_{i,a}$ is given as $\gamma_{i,a} = \beta_i - \phi + \psi_{i,a}$. In mathematical terms, the orientation of the flute is said to be in the position of Fig. 4(*a*) when the angular positions of the leading edge point satisfy the conditions of $\beta_i - \phi < \theta_{en}$ and $\gamma_{i,a} > \theta_{en}$.

Similarly, the expressions for the integration limits and the conditions at which these limits are applicable to all other orientations of the flute shown in Fig. 4 can be obtained as:

Case 1

$$\left.\begin{array}{c} \beta_i - \phi < \theta_{en} \\ \beta_i - \phi + \psi_{i,a} > \theta_{en} \end{array}\right\} \psi_{i,L} = 0, \quad \psi_{i,U} = \theta_{en} - (\beta_i - \phi)$$

Case 2

$$\left.\begin{array}{c} \beta_i - \phi \geq \theta_{en} \\ \beta_i - \phi + \psi_{i,a} \leq \theta_{en} \end{array}\right\} \psi_{i,L} = 0, \quad \psi_{i,U} = \psi_{i,a}$$

Case 3

$$\left.\begin{array}{c} \beta_i - \phi < \theta_{en} \\ \beta_i - \phi + \psi_{i,a} \leq \theta_{en} \end{array}\right\} \psi_{i,L} = \theta_{ex} - (\beta_i - \phi), \quad \psi_{i,U} = \psi_{i,a}$$

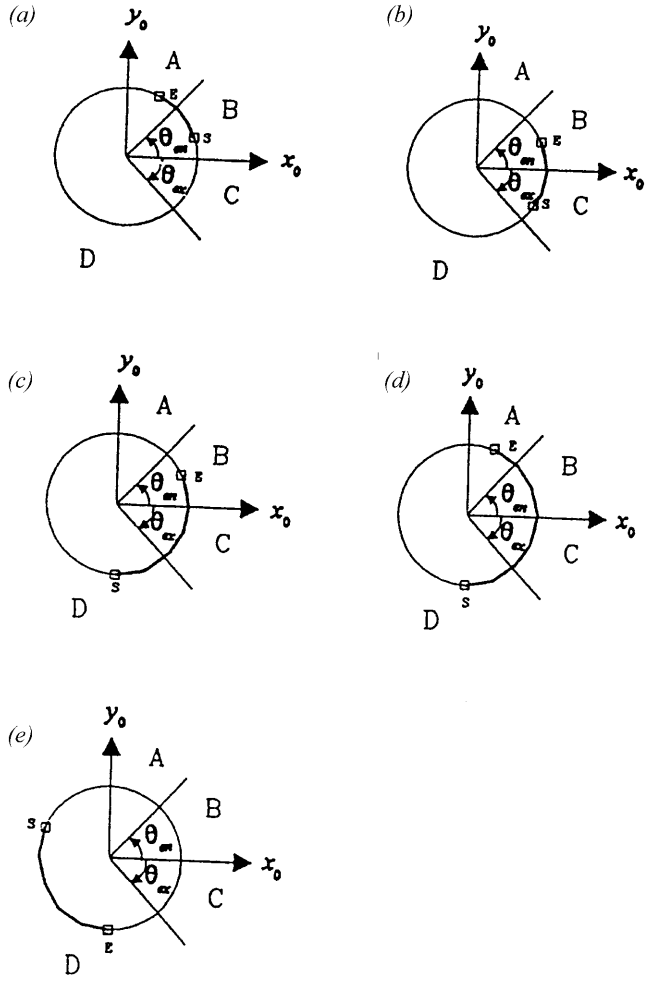

Fig. 4. Possible rotational positions of a flute with s = leading edge point, and E = angular position of a point on the flute that corresponds to the axial depth of cut d_a.

Case 4

$$\left.\begin{array}{c} \beta_i - \phi < \theta_{en} \\ \beta_i - \phi + \psi_{i,a} > \theta_{en} \end{array}\right\} \psi_{i,L} = \theta_{ex} - (\beta_i - \phi),$$
$$\psi_{i,U} = \theta_{en} - (\beta_i - \phi)$$

Case 5

Otherwise $\quad \psi_{i,L} = 0, \quad \psi_{i,U} = 0$

where cases 1 to 5 are based on the positions shown in Figs 4(*a*) to 4(*e*), respectively.

The above integration limits are valid for machining a plane surface with a constant radial depth of cut. However, if a sculptured surface must be produced, then, even when machining at a constant radial depth of cut, the axial depth of cut may vary along a contour of the surface. To determine these constantly varying cutting forces, the axial depth of cut must be constantly identified and be fed into the cutting force model. In the following section, an innovative method, capable of

estimating the axial depth of cut for a sculptured surface machining, is proposed.

3.4 Axial Depth of Cut Estimation

In order to estimate the axial depth of cut at any instant on a sculptured surface, the orientation of the cutter with respect to the sculptured surface at that instant of time must be known. There are several ways to *position* the cutter with respect to the surface. However, for rapid and efficient machining of the surface, the z_0-axis of the cutter must be placed in such a way that the direction of the axis is coincident with that of the surface normal. Figure 5 shows the cutter oriented in such a position.

As shown in the figure, the cutter has the flute length l_f. At an instant of time, it is located at point p_0 (x_0, y_0, z_0) on the surface. The cutter intersects with a plane at point $p(x,y,z)$. The position of the cutter at the end of the flute length is represented by point $p_1(x_1, y_1, z_1)$. Since the surface $\mathbf{r}(u,v)$ is represented in a parametric form in which u and v are the parameters of the surface, the unit surface normal $\mathbf{u}$ of the surface can be obtained by

$$\mathbf{u} = \frac{\mathbf{r}_u \times \mathbf{r}_v}{|\mathbf{r}_u \times \mathbf{r}_v|} \tag{19}$$

where $\mathbf{r}_u$ and $\mathbf{r}_v$ are partial derivatives of $\mathbf{r}$ with respect to the parameters u and v, respectively; and the term $|\mathbf{r}_u \times \mathbf{r}_v|$ in the equation is the magnitude of the surface normal $\mathbf{r}_u \times \mathbf{r}_v$. It is defined as $|\mathbf{r}_u \times \mathbf{r}_v| = \sqrt{((\mathbf{r}_u \times \mathbf{r}_v) \bullet (\mathbf{r}_u \times \mathbf{r}_v))}$. However, as illustrated in the figure, if vector p_0p_1 is to be on the same line as the extension of the unit surface normal $\mathbf{u}$, then the vectors p_0p_1 and $\mathbf{u}$ must satisfy the condition $\mathbf{u} \times p_0p_1 = 0$. This implies that $\mathbf{u}$ and p_0p_1 must be linearly dependent. Since for a regular surface, $u \neq 0$, p_0p_1 must be equal to a scalar (i.e. l_f) multiplied by $\mathbf{u}$. Or we can write

$$p_0p_1 = l_f\mathbf{u} \tag{20}$$

Equation (20) can be rewritten in the coordinates of point p_1 as

$$\{x,y,z\}^T = \{x_0,y_0,z_0\}^T + l_f\ \{u_x,u_y,u_z\}^T \tag{21}$$

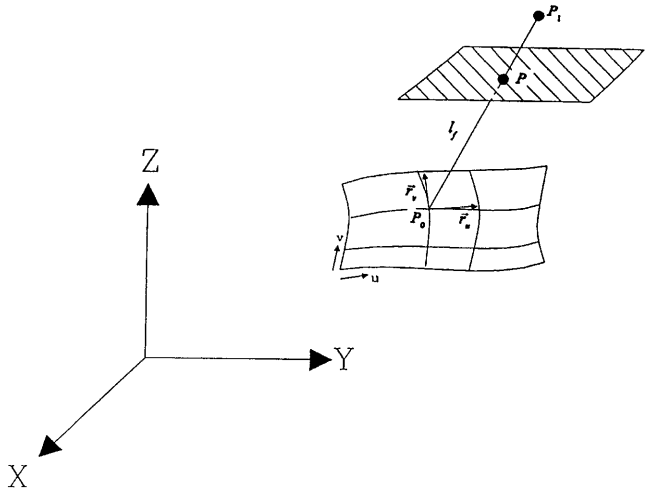

Fig. 5. The intersection of a cutter with a plane at point *P*.

where u_x, u_y and u_z are the three components of the unit surface normal $\mathbf{u}$ in the *X*, *Y* and *Z* directions of the *XYZ* coordinate system, respectively.

Similarly, with regard to the intersection point p of the cutter and the plane we can write

$$p_0p = gp_0p_1 \tag{22}$$

where g is a real variable. Again expanding this equation in its components, the following expression is obtained:

$$\{x_1,y_1,z_1\}^T = \{x_0,y_0,z_0\}^T + g\{x_1 - x_0, y_1 - y_0, z_1 - z_0\}^T \tag{23}$$

It can be seen from this equation that if $g = 0$, the point p coincides with the point p_0. On the other hand, if $g = 1$, then the point p is located at p_1. In other words, if the variable g in this Eq. is allowed to vary in the range of 0 to 1, $0 \leq g \leq 1$, then the point of intersection p will assume the position of any point on the line segment connecting p_0 and p_1. Physically, this constraint means that the axial depth of cut for the milling process cannot be larger than the flute length.

In implicit form, every plane in space is represented by an equation of the first degree in one or more of the variables *x*, *y*, and *z*. However, all these Eq. can be represented by a general expression

$$ax + by + cz = d \tag{24}$$

provided that *a*, *b*, *c*, and *d* are real numbers and *a*, *b*, and *c* are are not all zero.

Substituting Eq. (23) into (24) and simplifying, the general expression for the variable g at which the cutter and the plane intersect can be written as

$$g = \frac{d - a\,x_0 - b\,y_0 - c\,z_0}{a(x_1 - x_0) + b(y_1 - y_0) + c(z_1 - z_0)} \tag{25}$$

where the g varies in the range of 0 to 1.

If the shape of a workpiece is rectangular, then from Eq. (25) the g value for the cutter to intersect the *X*-plane of the workpiece is

$$g_x = \frac{d_x - x_0}{x_1 - x_0} \quad (0 \leq g_x \leq 1) \tag{26}$$

where d_x is the coordinate of intersection of the *X*-plane with the *X*-axis. Notice that in obtaining this equation, the equation of the plane $x = d_x$ has been applied to Eq. (25).

The equation that describes the *Y*-plane of the workpiece is $y = d_y$. Comparing this equation with Eq. (25), the g formula for the intersection of the cutter and the *Y*-plane becomes

$$g_y = \frac{d_y - y_0}{y_1 - y_0} \quad (0 \leq g_y \leq 1) \tag{27}$$

where d_y is again used to denote the coordinate of intersection of the *Y*-plane with the *Y*-axis.

Similarly, plugging the *Z*-plane equation, $z = d_z$, into Eq. (25), the g expression for this case is obtained as

$$g_z = \frac{d_z - z_0}{z_1 - z_0} \quad (0 \leq g_z \leq 1) \tag{28}$$

where d_z is the coordinate of intersection of the *Z*-plane with the *Z*-axis.

The main drawback of using an implicit form to describe a plane is that the equation that represents the plane represents an infinite plane. Therefore, for a rectangular workpiece a cutter with flute length l_f will either intersect one or more (at most 3 planes) planes of the workpiece at any instant. Among these intersection planes, the one that is most relevant for calculating axial depth of cut is the plane that first intersects the cutter. In fact, at that intersection the axial depth of cut is a minimum when compared with other possible intersections. In other words, the axial depth of cut that corresponds to the first intersection plane is determined by the following condition

$$d_a = \min\{\ |g_x p_0 p_1|\ |g_y p_0 p_1|\ |g_z p_0 p_1|\ \} \tag{29}$$

in which the first term in the brackets corresponds to the axial depth of cut with respect to the *X*-plane intersection. Similarly, the other two terms in the brackets are associated with the *Y*- and *Z*-plane intersections, respectively. However, among these three values in the equation, the one that is the minimum is the one that corresponds to the first intersection plane.

4. The Predictive Model Assessment on a Sculptured Surface Machining

Figure 6 shows a general sculptured surface to be machined from a rectangular shaped workpiece by using a milling cutter. The workpiece has dimensions of 7 mm in height, 20 mm in depth, and 45 mm in width. It is clear that in order to generate this surface from the workpiece, the axial depth of cut of the machining process must be continuously varied with time. Therefore, in order to calculate the predictive cutting forces, it must be estimated continuously and then fed back to the cutting-force model.

In this section a test is performed to assess the capability of the axial depth of cut estimation method as developed above for identifying the depth of cut for this machining operation. Comparisons of simulation results are also made against some data published in the literature to further validate the proposed cutting-force model. In addition, a cutting tool is designed by effectively arranging the helix angles of the tool using this predictive model as a guideline.

To perform the verification, a computer program was developed for simulation purposes. In the simulations, a 10 mm diameter HSS end mill has been used. The tool has four flutes with all the flute lengths being 19 mm. The normal rake angle for each flute is 5°. The tool is used to machine a 7075 aluminium workpiece. The cutting parameters, K_c and K_f, which were identified empirically by Wang et al. [6], are taken to be the nominal values in these simulations. The expressions of these identified parameters are as follows [6]:

$$K_c = 569.14\ (\bar{h}_c)^{-0.283}$$
$$K_f = 0.1468\ (\bar{h}_c)^{-0.364} \tag{30}$$

where the average chip thickness $\bar{h}_c$ is expressed as $\bar{h}_c = \int_{\theta_{en}}^{\theta_{ex}} f \cos\theta d\theta/(\theta_{ex} - \theta_{en})$. In addition, a sampling rate of 36 samples per revolution and a spindle speed of 1200 rev/min have been used in the simulations. The tool has been fed with a feedrate of 20 mm s^{-1} and the radial of cut of the tool is 10 mm. Gouging problems were not considered in the simulations.

Figure 7 shows the orientations and positions of the cutter along the path $v = 0.5$ of the surface. The orientations in the figure are plotted at every fifth position of the cutter. The cutting tolerance for generating this path is 0.02 mm. The positions as shown in the figure are obtained by using the adaptive cutting path generation algorithm [21]. However, the orientations and the axial depth of cut of the cutter are obtained by using the axial depth of cut estimation method proposed previously in this paper. In the figure, the depth of cut at any instant is determined by taking the corresponding distance between the cross symbols.

Figures 8 and 9 show the instantaneous cutting forces along the cutting path $v = 0.5$. The forces are obtained from the proposed predictive cutting-force model. The helix angles used in the simulations for these two figures are 5° and 30°, respectively. The observation of the force fluctuations in these figures indicates that as the helix angles increase the force in the *z*-direction also increases in tandem but it has little effect on the forces in the other two directions. Similar trends are also predicted by using the mechanics of cutting approach, even though the cutting parameters used in the prediction are different. However, the shortcoming of studying the effect of cutting parameter on the cutter, based on force fluctuations, is that it lacks the capability of describing in detail the intricate interactions of the cutting. Therefore, it was decided to use a statistical method (e.g. root mean square) to assist in the interpretation of the cutting phenomena.

Since the analysis would become very complicated if the effects of cutting parameters on the cutter were analysed for each component of cutting force, the analysis was carried out

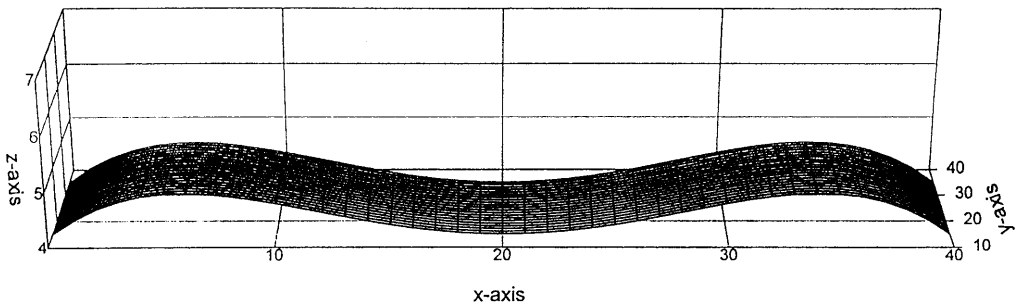

Fig. 6. A general shape of a sculptured surface.

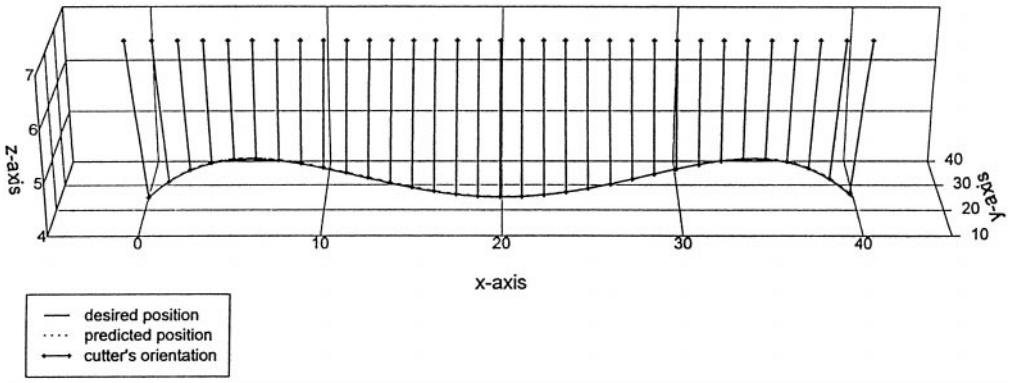

Fig. 7. Positions and orientations of a cutter along cutting path $v = 0.5$.

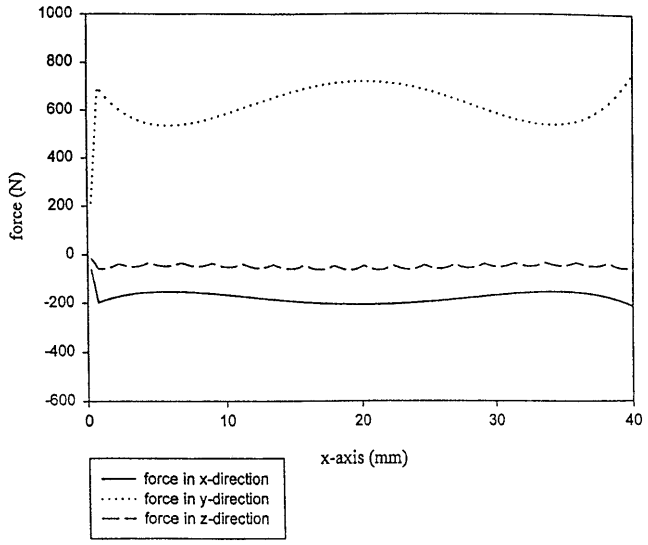

Fig. 8. Force responses for the full immersion of a cut along cutting path $v = 0.5$ with cutter helix angles of 5°, 5°, 5°, 5°.

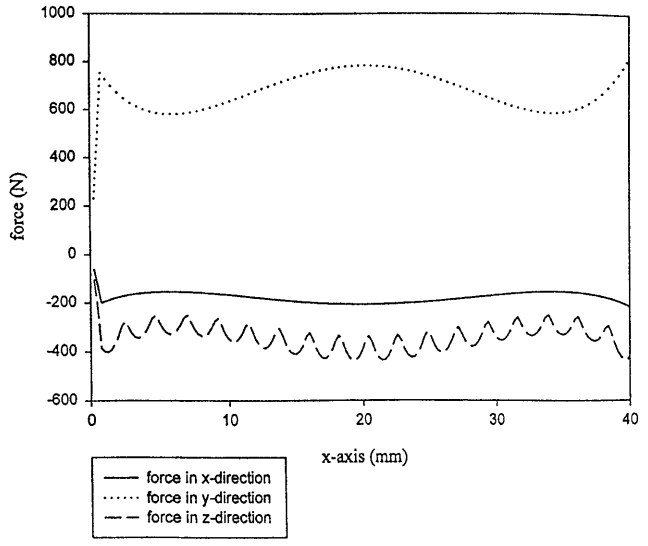

Fig. 9. Force responses for the full immersion of a cut along cutting path $v = 0.5$ with cutter helix angles of 30°, 30°, 30°, 30°.

based on the specific cutting force due only to the pressure component $F_{s,p}$. The pressure component is defined as

$$F_{s,p} = (R_{x,p}{}^2 + R_{y,p}{}^2 + R_{z,p}{}^2)^{1/2} \tag{31}$$

where $R_{x,p}$, $R_{y,p}$, and $R_{z,p}$ are the global cutting-force components which are due to the pressures of the chips on the rake surfaces of the cutter. Although the pressure component of the specific cutting force is not an instantaneous cutting force, it is a useful and effective method of investigating the effects of the cutting parameters on the cutter.

Table 1 shows the helix angle arrangements for a four-flute cutter with its corresponding root mean square value for specific cutting force due to pressures. As shown in Figs 8 and 9, the table also shows that as the helix angle of the flutes increases from 5° to 30°, the pressure-component (normal) specific cutting force will increase in tandem with the increase in angle in which the specific cutting force at 30° is 23.9% higher than that for 5°. However, the problem associated with this high normal specific cutting force is that it could cause the chips to adhere to the rake surfaces of the tool. This in turn could lead to the formation of built-up edges on the tool. On the other hand, if the cutting tool with a lower helix angle is chosen to machine a surface in which the radial engagement of the tool with the workpiece is less than full immersion, then the cutting force will increase to a maximum value and then rapidly drop to a minimum value. This sharp variation of force could act as an impact load which in turn could induce vibration in the cutter and/or machine tool.

The only way out of this dilemma is to design a tool that has a combination of different helix angles. In the case of a cutter with four flutes, the possible combinations of arrangements for the flutes with helix angles of 5° and 30° are,

Table 1. Helix angle arrangement and its corresponding specific cutting force for a cutter with four flutes.

Helix angle arrangement	Root mean square for specific cutting force due to pressure (N)
5°, 5°, 5°, 5°	628.5041
30°, 30°, 30°, 30°	778.8776
30°, 30°, 5°, 5°	701.0402
5°, 30°, 5°, 30°	689.3893

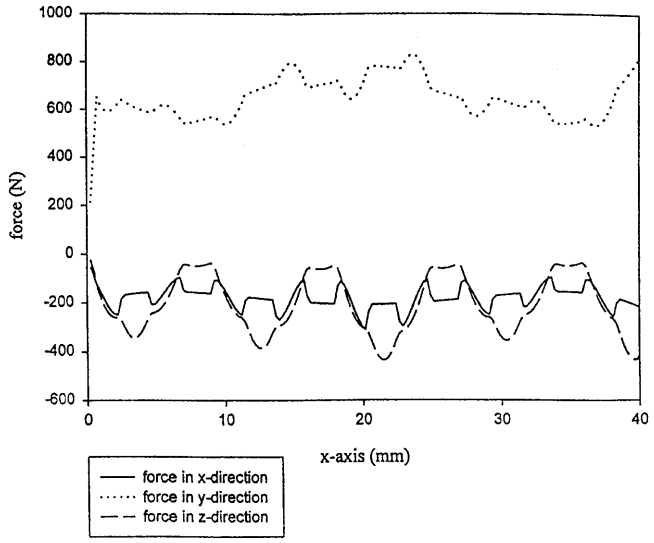

Fig. 10. Force responses for the full immersion of a cut along cutting path $v = 0.5$ with cutter helix angles of 30°, 30°, 5°, 5°.

[30,30,5,5] and [5,30,5,30]. However, according to the Table 1, the pressure component of the specific cutting force for the first arrangement is larger than for the second one. In fact, the percentage increase for the second arrangement compared to that with a cutter having a 5° helix angles, is 9.7%. The force fluctuations for these two new arrangements are shown in Figs 10 and 11, respectively.

5. Conclusion

The majority of work carried out in the past on the predictive cutting-force modelling of end milling processes was aimed at 2D planar surface generation. In this paper, a new comprehensive 3D predictive cutting-force model for milling sculptured surface parts has been proposed. The model was developed based on the mechanistic cutting approach and is presented in a closed-form format. As opposed to the empirical method commonly used in which the force information obtained is only valid for some specific cutting conditions, the proposed model provides a simple and generic means to determine the cutting force. It only requires identification of the coefficient of friction and the specific cutting pressure from tests.

In addition, the normal rake angle, which is usually missing in the existing models, has been included because it has a marked effect on the cutting horsepower calculation. Also, the proposed model considers the rake surface as an osculating plane which enables one to obtain 3D cutting-force expressions in two steps:

1. To determine the magnitude of the resultant cutting force acting on the flute.
2. To find the location of the line of action of the resultant force by using the principle of moments.

This procedure drastically reduces the mathematical work normally required in the derivation of cutting-force expressions. Moreover, this comprehensive model allows quantitative analyses of the effect of any parameters specified on the cutting performance of the tool. This in turn provides some guideline for further improvements of tool performance.

The simulation of machining a sculptured surface has shown the capability of the proposed estimation method to identify the axial depth of cut for machining. It also indicated that force responses of the model exhibit the same trends as those obtained from the mechanic cutting models reported in the literature. Further, the simulations have demonstrated the advantages of designing a tool with a combination of different helix angles having a cutting-force signature similar to the single helix angle counterparts.

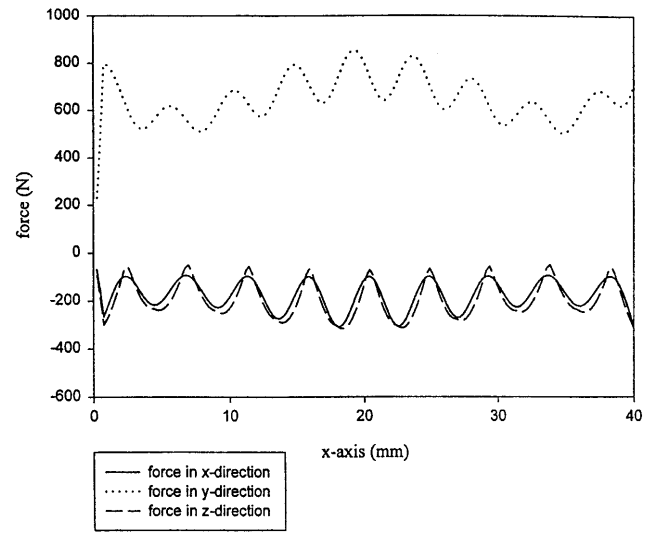

Fig. 11. Force responses for the full immersion of a cut along cutting path $v = 0.5$ with cutter helix angles of 5°, 30°, 5°, 30°.

Acknowledgement

The authors would like to acknowledge the partial support to this work from OBOR Grant R2375 and SME Grant 596–2205.

References

1. G. W. Vickers and K. W. Quan, "Ball-mills versus end-mills for curved surface machining", Transactions ASME Journal of Engineering for Industry, 111, pp. 22–26, 1989.
2. S. Ema and R. Davies, "Cutting performance of end mills with different helix angles", International Journal of Machine Tools and Manufacturing, 29(2), pp. 17–227, 1989.
3. S. Smith and J. Tlusty, "An overview of modeling and simulation of the milling process", Transactions ASME Journal of Engineering for Industry, 113, pp. 169–175, 1991.
4. A. E. Bayoumi, G. Yucesan and L. A. Kendall, "An analytic mechanistic cutting force model for milling operations: A theory and methodology", Transactions ASME Journal of Engineering for Industry, 116, pp. 324–330, 1994.
5. A. E. Bayoumi, G. Yucesan and L. A. Kendall, "An analytic mechanistic cutting force model for milling operations: A case study of helical milling operation", Transactions ASME Journal of Engineering for Industry, 116, pp. 331–339, 1994.
6. J. J. J. Wang, S. Y. Liang and W. J. Book, "Convolution analysis of milling force pulsation", Transactions ASME Journal of Engineering for Industry, 116, pp. 17–25, 1994.

7. G. Yucesan and Y. Altintas, “Prediction of ball end milling forces”, Transactions ASME Journal of Engineering for Industry, 118, pp. 95–103, 1996.
8. Y. Altintas and P. Lee, “Mechanics and dynamics of ball end milling”, Transactions ASME Journal of Manufacturing Science and Engineering 120(4), pp. 684–692, 1998.
9. A. J. P. Sabberwal, “Chip section and cutting force during the milling operation”, Annals CIRP, 10(3), pp. 197–203, 1961/1962.
10. M. E. Martellotti, “An analysis of the milling process”, Transactions ASME, pp. 677–700, November 1941.
11. J. Tlusty and P. MacNeil, “Dynamics of cutting forces in end milling”, Annals CIRP, 24, pp. 21–25, 1975.
12. R. I. King, Handbook of High Speed Machining Technology, Chapman and Hall, 1985.
13. W. A. Kline, R. E. DeVor and J. R. Lindberg, “The prediction of cutting forces in end milling with application to cornering cuts”, International Journal of Machine Tool Design and Research, 22(1), pp. 7–22, 1982.
14. R. E. DeVor, W. A. Kline and W. A. Zdeblick, “A mechanistic model for the force system in milling with application to machining airframe structure”, Manufacturing Engineering Transactions, 8, pp. 297–303, 1980.
15. W. A. Kline and R. E. DeVor, “The effect of runout on cutting geometry and forces in end milling”, International Journal of Machine Tool Design and Research, 23(2/3), pp. 123–140, 1983.
16. J. W. Sutherland and R. E. DeVor, “An improved method for cutting force and surface error prediction in flexible end milling systems”, ASME Journal of Engineering for Industry, 108, pp. 269–279, 1986.
17. J. W. Sutherland, “A dynamic model of the cutting force system in the end milling process”, ASME Sensor and Control for Manufacturing, PED 33, pp. 53–62, 1988.
18. K. D. Bouzakis, G. Metenitis and W. Koing, “Determination of the values of the technological parameters which are used to describe the time course of cutting force components in milling”, Annals CIRP 34(1), pp. 141–144, 1985.
19. E. J. A. Armarego and N. P. Deshpande, “Computerized predictive cutting models for forces in end-milling including eccentricity effects”, Annals CIRP, 38(1), pp. 45–49, 1989.
20. E. J. A. Armarego and R. H. Brown, The Machining of Metals, Prentice-Hall, 1969.
21. Y. J. Lin and T. S. Lee, “An adaptive tool path generation algorithm for precision surface machining”, 1998 ASME IMECE, MED-8, pp. 522–528, Anaheim, CA, November 1998.